Computer Modeling in Engineering & Sciences

Tech Science Press

DOI: 10.32604/cmes.2022.023454

check for updates

ARTICLE

Explicit Isogeometric Topology Optimization Method with Suitably Graded Truncated Hierarchical B-Spline

Haoran Zhu, Xinhao Gao, Aodi Yang, Shuting Wang, Xianda Xie and Tifan Xiong*

School of Mechanical Science and Engineering, Huazhong University of Science and Technology, Wuhan, 430074, China

*Corresponding Author: Tifan Xiong. Email: Xiongtf@hust.edu.cn

Received: 27 April 2022 Accepted: 30 June 2022

ABSTRACT

This work puts forward an explicit isogeometric topology optimization (ITO) method using moving morphable components (MMC), which takes the suitably graded truncated hierarchical B-Spline based isogeometric analysis as the solver of physical unknown (SGTHB-ITO-MMC). By applying properly basis graded constraints to the hierarchical mesh of truncated hierarchical B-splines (THB), the convergence and robustness of the SGTHB-ITO-MMC are simultaneously improved and the tiny holes occurred in optimized structure are eliminated, due to the improved accuracy around the explicit structural boundaries. Moreover, an efficient computational method is developed for the topological description functions (TDF) of MMC under the admissible hierarchical mesh, which consists of reducing the dimensionality strategy for design space and the locally computing strategy for hierarchical mesh. We apply the above SGTHB-ITO-MMC with improved efficiency to a series of 2D and 3D compliance design problems. The numerical results show that the proposed SGTHB-ITO-MMC method outperforms the traditional THB-ITO-MMC method in terms of convergence rate and efficiency. Therefore, the proposed SGTHB-ITO-MMC is an effective way of solving topology optimization (TO) problems.

KEYWORDS

Isogeometric topology optimization; moving morphable components; truncated hierarchical B-spline; suitably graded hierarchical mesh

1 Introduction

TO is an engineering optimization method that seeks the optimal material distribution in a prescribed design domain with specified conditions. In the last three decades, a series of TO methods have been proposed and evolved, including solid isotropic material with penalization [1,2], evolutionary structural optimization [3,4], and level set method (LSM) [5–7]. Most of these traditional TO methods use the finite element method (FEM) as the solver for the unknown physical field over the design domain, which suffers from numerical instability and geometric discretization errors, due to the low discontinuity between adjacent elements and the disconnection between computer aided design (CAD) and computer aided engineering (CAE).

Hughes et al. [8] proposed isogeometric analysis (IGA) to substitute the FEM method, which uses the CAD mathematical primitive to represent the field unknowns of the partial differential equations (PDEs). Since IGA has the advantages of high boundary continuity between adjacent elements and elimination of geometric discretization errors, Qian [9] used the relative density of control points

as design variables and embedded the physical design domain into a rectangular parametric design domain parametrized by the tensor product B-spline. Gao et al. [10] used ITO for the continuum structure using the enhanced density distribution function. Wang et al. [11] designed a new high-efficiency ITO, which improves the efficiency in three aspects: mesh scale reduction, acceleration strategy for the solver, and design variables reduction. Yu et al. [12] presented a multiscale ITO method, where the configuration and layout of microstructures are optimized synchronously. Zhao et al. [13] developed an ITO method for the design problems with an arbitrarily shaped design domain in the framework of T-spline based IGA. Chen et al. [14,15] applied the isogeometric boundary element based TO method to the design problems of acoustic structures for enhancing the sound-absorption performance. Due to the element-wise discreteness inherited from the variable density method, the ITO methods mentioned above easily get into trouble with the curse of dimensionality for generating accurate structural boundaries.

To resolve the issues that occurred in the variable density-based ITO methods, one alternative is the explicit TO method by Guo et al. [16] using MMC, which originated from the fact that the TO results can be viewed as the optimal distribution of a limited number of components. In the explicit TO method, the geometric characteristic parameters of a limited number of discrete components, e.g., the coordinates of the centroid and the inclination angle of a component, are treated as the design variables, by which the explicit geometric information of structural boundaries can be generated directly from the converged design variables. Zhang et al. [17] devised the finite-circle method to avoid the overlapping of components for the explicit TO method. Hou et al. [18] adopted the NURBS-based IGA method to obtain the structural response analysis and sensitivity analysis for the MMC-based explicit TO method. Then, an explicit ITO method is proposed with the geometric parameters of moving morphable voids (MMV) [19] treated as the design variables, which utilizes two mesh resolution schemes at different discretization levels. Gai et al. [20] proposed an explicit ITO method that uses the closed B-splines curves to describe the MMV. Zhang et al. [21] integrated the MMV method and the NURBS-based IGA to optimize the 3D shell structure. Since the sensitivity analysis of the explicit ITO depends on the structural boundaries, the accuracy of sensitivities around the structural boundaries determines the optimization accuracy of the explicit ITO method. However, due to the tensor product structure of B-splines, the analytical mesh of explicit ITO cannot perform local refinement of the boundary through the adaptive refinement technique, which leads to a severe contradiction between the analytical efficiency and optimization accuracy.

To resolve the contradiction between the efficiency and accuracy of the explicit ITO method, the problem of enforcement of global refinement for IGA mesh must be solved first. Currently, the main solutions for this issue are listed as: hierarchical B-splines [22], T-splines [14], LR-splines [23] and hierarchical box-splines [24]. Among these methods, the hierarchical B-spline is the most widely used one because of its provable linear independence and subdivision property [25]. Noël et al. [26] used truncated hierarchical B-splines to describe the parametrization of the level set function for LSM, which improved the accuracy of the structural boundaries with limited increased computational effort for the updating of design variables. Xie et al. [27] proposed an adaptive explicit ITO method based on hierarchical B-splines, which refines the isogeometric mesh associated with the regions near the optimized structural boundaries locally and achieves a significant balance between the computational efficiency and optimization accuracy. It has been stated that the THB is superior to the hierarchical B-splines in adaptive IGA because it improves the conditionality of the stiffness matrix and reduces the bandwidth of the stiffness matrix [28]. Subsequently, Xie et al. [29] put forward the fully adaptive explicit ITO method with more advanced computing efficiency in terms of truncated hierarchical B-splines, where the isogeometric mesh is locally refined and coarsened simultaneously and the corresponding basis function space recovers the property of partition of unity. However, in the current

adaptive explicit ITO method, tiny holes are easily observed in the optimized structures, which should be eliminated for the benefits of both the numerical robustness of the optimization process and the manufacturing of optimized structures. The underlying reason for the aforementioned weaknesses of the adaptive explicit ITO method is that the analytical accuracy of the THB-based IGA method is deteriorated in the regions of structural boundaries, resulting from the non-constrained hierarchical differences between the non-vanishing THB basis functions.

As pointed out in [30], the admissible mesh can effectively improve the accuracy of the THB-based IGA method. To overcome the shortcoming of the current adaptive explicit ITO method, the present work proposes an advanced adaptive explicit ITO method using MMC in terms of suitably graded truncated hierarchical B-spline (SGTHB-ITO-MMC). Based on the marking strategy proposed in [31], this work develops a constrained marking strategy for imposing the suitably graded constraint on the hierarchical mesh, which enlarges the set of active elements marked to be refined and shrinks the set of deactivated elements marked to be coarsened. With the imposed suitably graded constraint, the accuracy and robustness of the adaptive explicit ITO method are improved. Besides, to further improve the efficiency in computing the TDF values for the hierarchical mesh, we designed an improved TDF calculation strategy for the deletion of the micro components and the local TDF computing strategy for the Gaussian quadrature points.

The rest of this paper is organized as follows: Section 2 "Suitably graded THB based ITO using MMC" introduces the basic theory of the SGTHB-ITO-MMC method, including the definitions corresponding to THB and admissible hierarchical meshes. The optimization model and marking strategy as well as the improved TDF calculation strategy for SGTHB-ITO-MMC are introduced in detail in Section 3 "Optimization model of SGTHB-ITO-MMC". Section 4 "Overview scheme for SGTHB-ITO-MMC" presents an overall procedure for SGTHB-ITO-MMC. In Section 5 "Numerical examples", the effectiveness of SGTHB-ITO-MMC is validated by several 2D and 3D benchmarks. Finally, this work is concluded in Section 6 "Conclusions".

2 Suitably Graded THB Based ITO Using MMC

This section provides the theoretical foundation for the proposed SGTHB-ITO-MMC, which mainly includes the following two aspects: the construction of THB and the related concepts of admissible hierarchical meshes.

2.1 Truncated Hierarchical B-Splines

2.1.1 Hierarchical B-Spline Spaces

For a given knot vector $\Xi = \{\xi_1, \xi_2, \cdots, \xi_{n+p+1}\}$, n and p represent the number of control points and the order of basis function, respectively. Supposing that several function spaces of B-spline are nested: $V^0 \subset V^1 \subset \ldots \subset V^{n-1}$, these nested spaces are obtained by a sequence of knot vectors $\{\Xi^0, \Xi^1, \ldots, \Xi^{N-1}\}$ and defined on an initial domain Ω^0. For multivariate case, V^l $(l = 1, 2, \ldots, N-1)$ is constructed by the tensor product structure of the univariate basis function space with the knot vector Ξ^l bisected from Ξ^0 l-times. Then, the knot intervals constituting a mesh $\boldsymbol{Q}^l$ and an arbitrary knot interval are referred to as an element of level l. Define $\Omega^0 \supseteq \Omega^1 \supseteq \ldots \supseteq \Omega^{N-1}$ as a nested sequence of domains, where Ω^l is the domain of level l and represents the union of the elements on $l-1$ level marked to be subdivided. Subsequently, a hierarchical mesh **HE** is made up of active elements on different levels and is defined as:

$$\mathbf{HE} = \{Q \in \Gamma^l, l = 0, \cdots, N-1\} \tag{1}$$

where Γ^l represents the union of active cells of level l with $Q \subset \Omega^l \wedge Q \not\subset \Omega^{l+1}$.

Once the hierarchical mesh **HE** is determined [32], the corresponding hierarchical B-spline function space can be constructed by the following steps:

- Initialization: $\mathcal{H}(\mathbf{HE})^0 = \{\beta \in B^0 : \text{ supp } \beta \neq \varnothing\}$;
- A recursive formula: $\mathcal{H}(\mathbf{HE})^{l+1} = \mathcal{H}_A^{l+1} \cup \mathcal{H}_B^{l+1}, l = 0, 1, \ldots, N-2$,
  where $\mathcal{H}_A^{l+1} = \{\beta \in \mathcal{H}(\mathbf{HE})^l : \text{ supp } \beta \not\subset \Omega^{l+1}\}$ and $\mathcal{H}_B^{l+1} = \{\beta \in B^{l+1} : \text{ supp } \beta \subseteq \Omega^{l+1}\}$,
  with $\text{supp } \beta = \{x : \beta(x) \neq 0 \wedge x \in \Omega^0\}$;
- $\mathcal{H}(\mathbf{HE}) = \mathcal{H}(\mathbf{HE})^{N-1}$.

2.1.2 Truncated Operation

The hierarchical B-splines basis functions are inevitably spanning the active elements belonging to different levels, which results in the lacking of the essential property of partition of unity for numerical analysis. To recover this important property, a truncated operation should be applied to the two-scale relationship existing in the basis functions of hierarchical B-splines on two consecutive levels, which is formulated as:

$$trunc^l(s) = \sum_{\beta \in B^{l+1}, \text{supp } \beta \notin \Omega^{l+1}} c_\beta^{l+1}(s)\,\beta,$$

$$\text{where } s = \sum_{\beta \in B^{l+1}} c_\beta^{l+1}(s)\,\beta, s \in V^l \tag{2}$$

where $trunc^l(s)$ is a truncated active basis function of s of level l, $c_\beta^{l+1}(s)$ is termed as the coefficient of β belonging to level $l+1$. Therefore, the THB function space $\mathscr{H}\mathscr{T}$ can be generated by the extended truncated operation for active basis functions on non-consecutive levels, as follows:

$$TRUNC^{l+1}(s) = trunc^N\left(trunc^{N-1}\left(\ldots\left(trunc^{l+1}(s)\right)\ldots\right)\right)$$

$$\mathcal{HT}(\mathbf{HE}) = \left\{TRUNC^{l+1}(s) : s \in \boldsymbol{B}^l \cap \mathcal{H}(\mathbf{HE}), l = 0, \cdots, N-2\right\} \cup \left\{s^{N-1} \in \left(\boldsymbol{B}^{N-1} \cap \mathcal{H}(\mathbf{HE})\right)\right\} \tag{3}$$

An illustration of hierarchical B-splines basis function space and its corresponding THB basis function space are shown in Fig. 1.

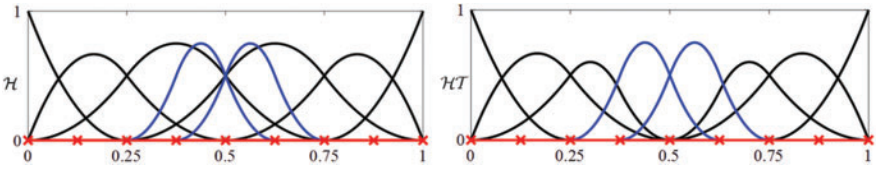

Figure 1: Illustration of hierarchical B-splines space $\mathscr{H}$ **(HE)** and THB space $\mathscr{H}\mathscr{T}$ **(HE)**

2.2 *Suitably Graded Admissible Meshes*

To ensure that the hierarchical computational mesh of the proposed SGTHB-ITO-MMC model satisfies the specified suitably graded constraints, this section reviews the key definitions related to the admissible hierarchical mesh for THB [30,33], which are elaborated as follows.

Definition 2.1. For an admissible mesh **HE** of class m, the truncated basis functions in THB basis function space $\mathscr{H}\mathscr{T}$ **(HE)** taking nonzero values over any active element belong to no more than m successive levels, as shown in Fig. 2.

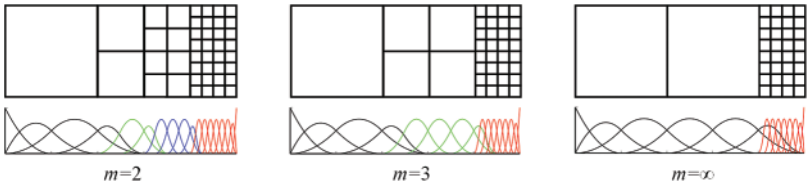

Figure 2: Admissible hierarchical meshes and their associated THB basis function with three different suitably graded constraints

Definition 2.2. The multilevel support extension of any an element $Q \in \boldsymbol{Q}^l$ on level k $(0 \leq k \leq l)$ is defined as:

$$S(Q,k) = \left\{Q' \in \boldsymbol{Q}^k : \exists \beta \in \boldsymbol{B}^k, \text{supp}\,\beta \cap Q' \neq \varnothing \wedge \text{supp}\,\beta \cap Q \neq \varnothing\right\} \tag{4}$$

Definition 2.3. For a level l element Q, the refining neighborhood N_r (**HE**, Q, m) with admissibility m is defined as:

$$N_r(\mathbf{HE}, Q, m) = \left\{Q' \in \mathbf{Q}^{l-m+1} : Q'' \in S(Q, l-m+2), Q'' \subseteq Q'\right\} \tag{5}$$

Definition 2.4. For a level l element Q, the coarsening neighborhood N_c (**HE**, Q, m) with admissibility m is defined as:

$$N_c(\mathbf{HE}, Q, m) = \left\{Q' \in \mathbf{Q}^{l+m} : Q'' \in \mathbf{Q}^{l+1} \wedge Q'' \in Q, \text{with } Q' \in S(Q'', l+1)\right\} \tag{6}$$

Fig. 3 illustrates the definitions shown in Eqs. (4) and (5) as well as (6), which is vital to implement the suitably graded refinement and coarsening for the THB hierarchical mesh. The green elements in Fig. 3 represent adjacent elements of level 0 for the active element Q (marked as yellow), which is an essential parameter for the admissible refinement and coarsening algorithms to check whether the active element Q violates the suitably graded constraint or not. The combination of Eqs. (4) and (5) can determine the grid cells adjacent to the marked refining active cell that should be refined locally to satisfy the specified admissible elements, and the combination of Eqs. (4) and (6) can determine the coarsening cells during the admissible coarsening of the hierarchical mesh.

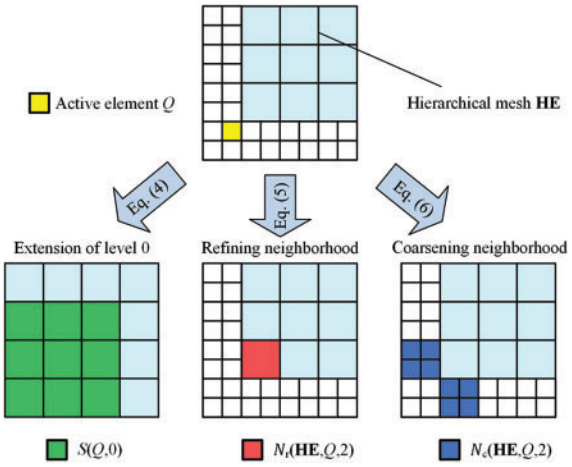

Figure 3: Illustration of the multilevel support extended domain S, refined neighboring domain N_r, and coarsened neighboring domain N_c for an active element Q

3 Optimization Model of SGTHB-ITO-MMC

The mathematical optimization model of the SGTHB-ITO-MMC method is firstly proposed in this section. Then, the constrained marking strategy is devised by integrating the fully adaptive marking strategy with the suitable constraint imposed on the hierarchical mesh, which controls the local refinement and coarsening of the hierarchical mesh for SGTHB-ITO-MMC. Finally, the improved TDF calculation strategy is described to improve the efficiency of SGTHB-ITO-MMC.

3.1 Mathematical Optimization Model

According to the optimization model presented in [27], the optimization model of SGTHB-ITO-MMC is formulated as:

$$\text{find } \boldsymbol{d} = \left(\boldsymbol{d}_1^{\mathrm{T}}, \boldsymbol{d}_2^{\mathrm{T}}, \ldots, \boldsymbol{d}_N^{\mathrm{T}}\right)^{\mathrm{T}}, \boldsymbol{u}(x)$$

$$\text{minimize } C = \sum_{l=0}^{N_0-1} \sum_{e=1}^{N_e^l} \left(\boldsymbol{u}_e^l\right)^{\mathrm{T}} \overline{\boldsymbol{K}}_e^l \boldsymbol{u}_e^l \left(\boldsymbol{u}_e^l = \tilde{\boldsymbol{C}}_e^l \boldsymbol{u} \text{ for } e = 0, 1, \ldots, N_e^l\right)$$

s.t.

$$\boldsymbol{K} \cdot \boldsymbol{u} = \boldsymbol{F}$$

$$\text{with } \boldsymbol{K} = \left(\sum_{l=0}^{N_0-1} \left(\tilde{\boldsymbol{C}}^l\right)^T \sum_{e=1}^{N_e^l} \overline{\boldsymbol{K}}_e^l \tilde{\boldsymbol{C}}^l\right), \quad \sum_{l=0}^{N_0-1} \sum_{e=1}^{N_e^l} \rho_e^l V_e^l \le \overline{V}, \quad \boldsymbol{d} \subset \mathcal{U}_d \tag{7}$$

In the above formula, $\boldsymbol{d}$ represents explicit geometric design variables of MMC, which are similar to the shape explicitly expressed by seven parameters, $\boldsymbol{u}(x)$ is the displacement vector of the active control points of the admissible hierarchical mesh, C denotes the objective function of the optimization model representing the structural compliance, $N_0 - 1$ is the maximum level of the hierarchical mesh, N_e^l denotes the number of active elements of level l, $\boldsymbol{u}_e^l$ is the local displacement vector of the e-th active element belonging to level l, $\overline{\boldsymbol{K}}_e^l$ and $\boldsymbol{K}$ represent the stiffness matrix of the e-th active element of level l, and the global stiffness matrix, respectively, which are related by the transformation matrix $\overline{\boldsymbol{C}}^l$ with $\tilde{\boldsymbol{C}}_e^l$ collecting the components of $\overline{\boldsymbol{C}}^l$ non-vanishing on the e-th active element of level l, $\boldsymbol{F}$ represents the vector of external force, ρ_e^l is the relative material density of the e-th element of level l, $\overline{V}$ and V_e^l represent the volume constraint limit and the elemental volume of the e-th active element of level l, and $\mathcal{U}_d$ denotes the admissible space for the explicit geometric design variables.

It should be noted that the ersatz material model and the sensitivity analysis are rather straightforward for SGTHB-ITO-MMC, which can be referred to [29] and are not provided in this work for brevity. In this work, the concept of suitably graded constraint is implemented by altering the marking strategy of hierarchical mesh, which can be presented in the next section.

3.2 Constrained Marking Strategy

To implement the adaptivity of hierarchical mesh under the specified suitably graded constraint, a constrained marking strategy is developed. The proposed marking strategy in this work consists of three aspects: triggering strategy, local refining, and local coarsening strategies under suitably graded constraints, where the triggering strategy is calculated in the same way as the one proposed in [29]. The local refining strategy and the local coarsening strategy are divided into two stages: (1) initial marking

based on TDF values at Gaussian quadrature points; (2) updating the initial marked set under suitably graded constraints.

3.2.1 Local Refined Marking Strategy

Once the marking strategy is triggered, the initial local refining of the marking strategy formulated as Eq. (8) finds the elements to be refined by resorting to the topological description function (TDF) values of the active element Gaussian points, as indicated by the green elements shown in Fig. 4.

$$M_{ref,e}^{lev} = \begin{cases} 1, \text{ if } \exists \left|\varphi_{g,e}^{lev}\right| \le t_{ref}^{lev} \left(g = 1, \ldots, n_{gp}\right) \\ 0, \text{ otherwise} \end{cases}$$

$$\text{with} \qquad lev = 0, 1, \ldots, N_0 - 1 \qquad \text{and} \qquad e = 1, 2, \ldots, N^{l} \tag{8}$$

where $M_{ref,s}^{le}$ represents the flag determining whether the e-th element of the lev-th level is to be refined or not, $\varphi_{s,e}^{le}$ is the TDF value of the s-th Gaussian quadrature point of the e-th active element of the l-th level, t_{ref}^{le} is the tolerance limit describing the neighborhood of the structural boundaries.

If the initial refining element set marked to be refined is obtained, the updating procedures for the initial marked set are described in Algorithms 1 and 2 to fulfill the specified suitably graded constraint during the local refinement of the hierarchical mesh. Algorithm 1 takes the original hierarchical mesh **HE**, THB basis function space $\mathscr{T}$, and the set of initial refining for marking elements M_{ref} as well as the specified suitably graded constraint m as the input parameters, which plays a role in updating the marked elements in a manner of level-by-level and the entry point for the Algorithm 2. Then, Algorithm 2 refines the elements that do not satisfy the hierarchical constraints by checking the refinement neighborhood of each initial refining element belonging to M_{ref}, which obtains from Eq. (8). These elements are added to the M_{ref}, thus ensuring that the hierarchical mesh still satisfies the suitably graded requirements of the hierarchical mesh. The newly added elements marked to be refined are shown in the green striped element in Fig. 4.

Algorithm 1 updating_refining_set

Input: **HE**, $\mathscr{T}$, M_{ref}, m
Output: M_{new_ref}
1: **for** $lev = 1$: numel (M_{ref}) **do**
2: $M_{new\_ref} \leftarrow$ mark_recursive (**HE**, $\mathscr{T}$, M_{ref}, lev, m)
3: **end for**

Algorithm 2 mark_recursive

Input: **HE**, $\mathscr{T}$, M_{ref}, lev, m
Output: M'_{ref}
1: $neighbors \leftarrow$ hspace_get_H_neighborhood ($\mathscr{T}$, **HE**, lev, M_{ref}^{lev}, m)
2: **if** $neighbors! = \varnothing$ **then**
3: $k = lev - m + 1$
4: $M_{ref}^{k} \leftarrow M_{ref} \cup neighbors$
5: $M'_{ref} \leftarrow$ mark_recursive (**HE**, $\mathscr{T}$, M_{ref}^{k}, lev, m)
6: **end if**

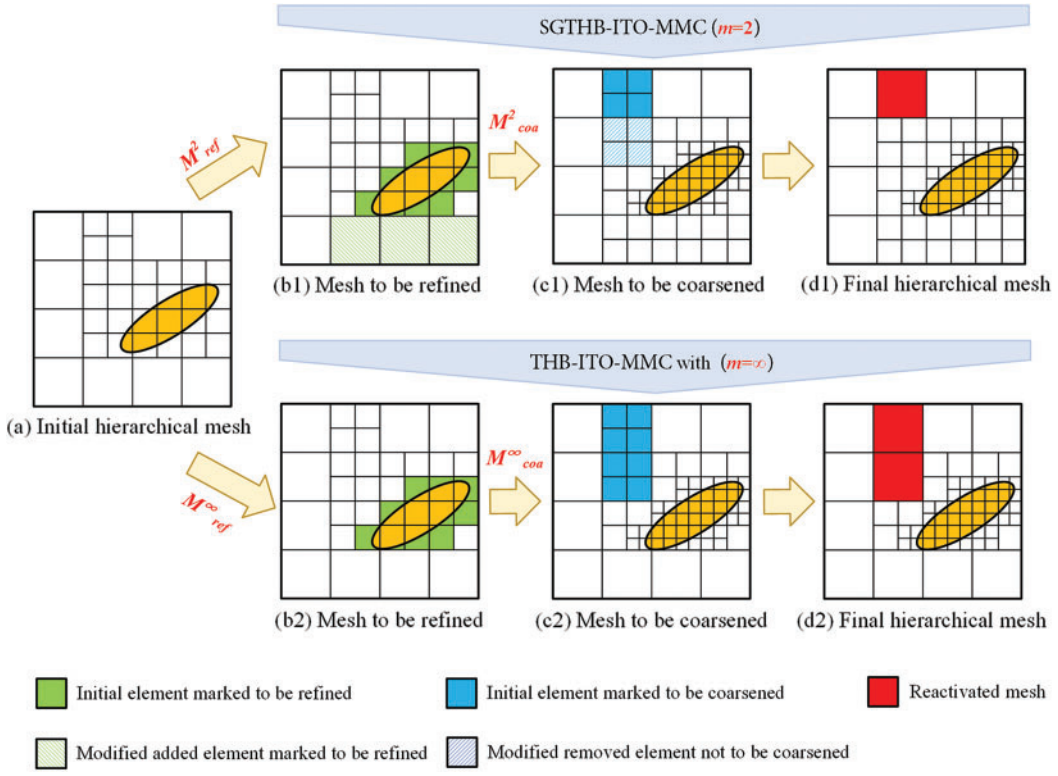

Figure 4: Illustration of the differences in the variations of the hierarchical mesh between different suitably graded constraints with $m = 2$ and $m = \infty$: (a) Initial hierarchical mesh; (b1) Mesh to refined; (c1) Mesh to coarsened; (d1) Final hierarchical mesh; (b2) Mesh to refined; (c2) Mesh to coarsened; (d2) Final hierarchical mesh

3.2.2 Local Coarsened Marking Strategy

When the local refinement of the hierarchical mesh is accomplished, the elements away from the structural boundaries should be marked to be coarsened for SGTHB-ITO-MMC. Similar to the refining strategy, the local coarsening strategy is also divided into two stages: (1) obtaining the initial marking set to be coarsened; (2) updating the coarsened element set. According to the TDF values of the Gaussian quadrature points of the children for each deactivated element, the status of that deactivated element to be refined or not is determined as follows:

$$M_{coa,b}^{lev} = \begin{cases} 1, & \text{if } \forall \varphi_{u,v,b}^{lev+1} > t_{coa}^{lev} || \forall \varphi_{u,v,b}^{lev+1} < -t_{coa}^{lev} \\ 0, & \text{otherwise} \end{cases} \quad \left(u = 1, \ldots, n_{gp} \quad \text{and} \quad v = 1, \ldots, 4\right)$$

$$\text{with } b = 1, 2, \ldots, N_{ad,D}^{l} \text{ and } lev = 0, 1, \ldots, N_0 - 2 \tag{9}$$

where $M_{coa,b}^{lev}$ denotes the flag that determines the b-th deactivated element of the lev-th level in the set of admissible deactivated elements $\boldsymbol{E}_{ad,D}^{lev}$ to be coarsened or not with $\boldsymbol{E}_{ad,D}^{lev}$ defined by Eq. (10), $\varphi_{u,v,b}^{lev+1}$ denotes the TDF value of the u-th Gaussian quadrature point of the v-th child for the b-th deactivated element of lev-th level, t_{coa}^{l} is the limit value used to define the regions far away from the structural boundaries.

$$\boldsymbol{E}_{ad,D}^{lev} = \left\{ e \in \left(\boldsymbol{E}_{D}^{lev} / \boldsymbol{E}_{refine}^{lev} \right) : \forall children\,(e) \in \boldsymbol{E}_{A}^{lev+1} \right\} \tag{10}$$

where $\boldsymbol{E}_D^{lev}$ is the union of deactivated elements of *lev*-th level, $\boldsymbol{E}_{refine}^{lev}$ and $\boldsymbol{E}_A^{lev+1}$ are the union of active elements of level *lev* and *lev*+1, *children*(*e*) denotes all children of a deactivated element which belongs to the subtraction between $\boldsymbol{E}_D^{lev}$ and $\boldsymbol{E}_{refine}^{lev}$.

Then, the marked coarsened set is updated by the procedures presented in Algorithm 3 to guarantee the admissible requirement resulting from the suitably graded constraint. In Algorithm 3, the deactivated element should be reactivated and its children should remain unchanged in the hierarchical mesh, if its coarsening neighborhood with admissibility m is null; otherwise, that deactivated element should be removed from the reactivated element set M_{coa}, which is indicated by the blue stripes in Fig. 4.

Algorithm 3 hmsh_coarsen_admissible

Input: HE, $\mathscr{T}$, M_{coa}, m
Output: HE, *new_deactivated_elements*, M'_{coa}
1: **for** $Q \in \mathcal{R}_c$ **do**
2: **if** N_c(**HE**, Q, m) == $\varnothing$ **then**
3: $Q_c \leftarrow$ get_children (Q)
4: update **HE** by activating Q and removing its children Q_c
5: $M'_{coa} \leftarrow M_{coa} \cup Q$
6: **end if**
7: **end for**

Fig. 4 shows the variations of the hierarchical mesh during the complete mesh adaptivity under the suitably graded constraints with $m = 2$ and $m = \infty$, from which can be observed that the constrained marking strategy proposed in this work generates smaller and controllable differences in hierarchical level between adjacent active elements.

3.3 Improved TDF Calculation Strategy for SGTHB-ITO-MMC

To improve the computational efficiency of SGTHB-ITO-MMC method, this work proposes the following strategy for the benefit of accelerating the calculation of TDF values for the hierarchical mesh. On the one hand, the computing complexity of TDF is reduced by removing the unnecessary TDF computing associated with micro components, with the micro components removed from the design space. On the other hand, the TDF generation is calculated locally inconsistent with the hierarchy feature of the hierarchical mesh.

3.3.1 Dimensionality Reduction Strategy

To avoid the numerical singularity, the lower limit of the geometric design variables of MMC is set to an extremely small positive value. It can lead to the numerical phenomenon that the islanding micro component exists in the optimized structure, as shown in Fig. 5.

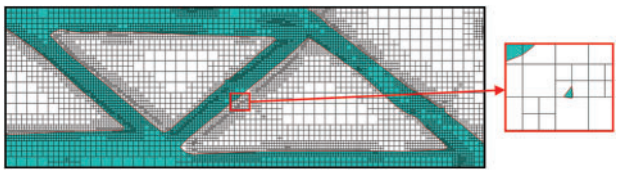

Figure 5: Illustration of the occurrence of islanding micro component in the optimized result

These islanding micro components result in the continuously refined mesh around them and that leads to the increasing deteriorative mesh quality. It also results from an excessive number of degrees of freedom, which decreases the computational efficiency of IGA. Therefore, it is necessary to reduce the dimensionality of the geometric design space by removing the design variables associated with micro components in the optimization process. If a component satisfies the requirements of Eq. (11) in the specified consecutive iterations, the associated micro-component is removed from the design space of SGTHB-ITO-MMC.

$$L_i < \varepsilon || t_{1i} < \varepsilon || t_{2i} < \varepsilon || t_{3i} < \varepsilon \tag{11}$$

where L_i is the half length of the i-th component, t_{1i} and t_{2i} as well as t_{3i} is the half thickness of the i-th component at locations of two ends and middle, ε is the user-defined size threshold for determining the micro components.

3.3.2 Local Computing Strategy

Apart from the micro components, the redundant TDF calculation also resulted from the way of calculating the TDF values for determining the ersatz material model. In this model, the Gaussian points of the hierarchical mesh inside the active elements are properly graded, and the Gaussian quadrature points do not span different levels of active elements, which enables the local updating of TDF for the hierarchical mesh. Besides, the active elements away from the structural boundaries do not require calculating the TDF values of the Gaussian quadrature points, since SGTHB-ITO-MMC is an essentially boundary-driven TO method. Therefore, the values of TDF of a structural component can be calculated only by Gaussian quadrature points near the boundary of the component, as shown in Fig. 6.

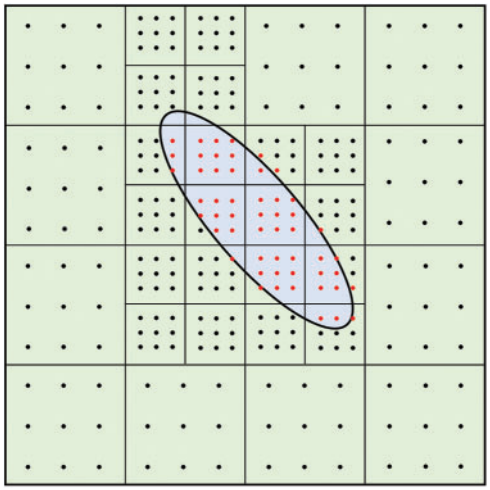

Figure 6: Active Gaussian points (red) and inactive Gaussian quadrature points (black) when φ_n setting 0

In the proposed local TDF computing strategy, the set of active Gaussian quadrature points is defined in Eq. (12) for the hierarchical mesh.

$$\boldsymbol{P}_{active} = \left\{ \varphi_i^j \geq \varphi_n, j \in \boldsymbol{P} \right\} \tag{12}$$

where $\boldsymbol{P}_{active}$ is the n-th level mesh, φ_i^j is the TDF value of the i-th component at the j-th Gaussian quadrature point, φ_n is the TDF value threshold for the n-th level, and $\boldsymbol{P}$ is the point set of Gaussian quadrature points, which are dynamically altered with the adaptivity of the hierarchical mesh.

4 Overview Scheme for SGTHB-ITO-MMC

This section mainly describes the execution process of the SGTHB-ITO-MMC method. The execution flow of the SGTHB-ITO-MMC method is shown in Fig. 7, which mainly consists of six modules: input module, mesh adaptivity module, ersatz material model module, IGA module, sensitivity analysis module, and output module.

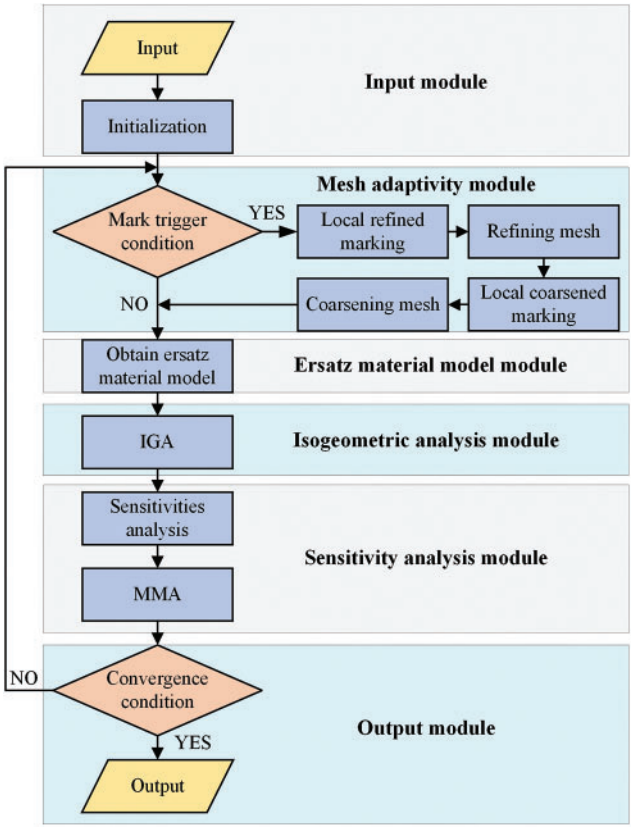

Figure 7: Illustration of the flowchart of the SGTHB-ITO-MMC algorithm

Among them, the input module takes the mathematical model parameters in Section 3.1 "Mathematical optimization model" as the input parameters and initializes these parameters. The mesh adaptivity module performs the local refinement and coarsening of hierarchical mesh based on the constrained marking strategy as described in Section 3.2 "Constrained marking strategy". In the ersatz material model module, the improved TDF calculation strategy presented in Section 3.3 "Improved TDF calculation strategy for SGTHB-ITO-MMC" is used to improve the efficiency of determining the material physical properties for all active elements. IGA module is represented as the IGA, which is used to calculate the structural responses under the hierarchical mesh. For the sensitivity analysis module, SGTHB-ITO-MMC uses the method of moving asymptotes (MMA) as the optimizer for updating the geometric design variables to achieve the minimization of the structural compliance. Finally, the output module is used to output the optimized explicit geometric parameters of all MMC.

5 Numerical Examples

Four numerical examples are used to demonstrate the effectiveness of the SGTHB-ITO-MMC framework with an improved TDF calculation strategy, which is running on MATLAB R2021a with Windows 10 as the software operating system, Intel (R) Core (TM) i5-10210U CPU @ 1.60 GHz–2.11 GHz and 16 GB of RAM as the hardware system. These examples adopted MMA as the optimizer. Young's modulus E and Poisson's ratio υ are set to 1 and 0.3 as the constant physical values for solid material, respectively. Besides, SGTHB-ITO-MMC with $m = \infty$ is identical to the THITO-MMC method presented in [29].

Through the Messerschmidt-Bolkow-Blohm beam (MBB) problem, Section 5.1 "MBB beam problem" verifies the validity of the suitably graded constraint in improving the optimized results and convergence, and the effectiveness of the improved TDF calculation strategy in enhancing the efficiency for SGTHB-ITO-MMC. In Section 5.2 "Short beam problem", the effectiveness of SGTHB-ITO-MMC and the improved TDF calculation strategy are validated at two different scales of geometric design space. Finally, the SGTHB-ITO-MMC method is extended to the 3D problem in Section 5.3 "3D cantilever beam problem".

5.1 MBB Beam Problem

This section chooses the MBB beam as the first example to verify the effectiveness of SGTHB-ITO-MMC. Fig. 8 depicts the problem configurations and initial design of MMC, where the aspect ratio of the rectangular design domain is 3:1 and the design domain is initially divided into 45×15 uniform IGA mesh. Moreover, the upper limit of the volume fraction is 0.4 for solid material. Maximum iterations equaling 300 and the convergence criterion are used to control the termination of the proposed optimization algorithm.

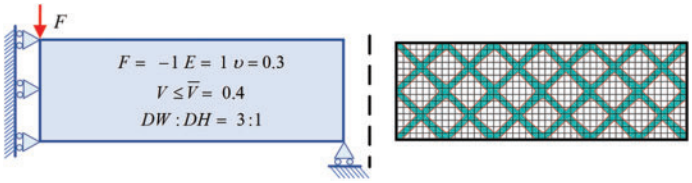

Figure 8: Problem model and the initial design for MBB beam problem

Fig. 9 presents the optimized results between different SGTHB-ITO-MMC with $m = 2$, $m = 3$, and $m = \infty$, where the tiny holes that occurred in the converged design of SGTHB-ITO-MMC with $m = \infty$ are eliminated in these results by SGTHB-ITO-MMC with $m = 2$, $m = 3$ and the iterative steps is increasing reduced as the stricter suitably graded constraint imposed on the hierarchical mesh.

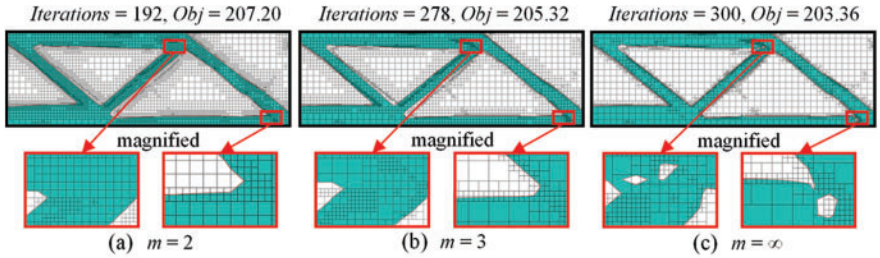

Figure 9: Optimized results by SGTHB-ITO-MMC with (a) $m = 2$, (b) $m = 3$, and (c) $m = \infty$

The convergence histories and the variations of the number of DOFs are illustrated in Fig. 10, where *Iterations* and *Obj* are referred to as the number of iteration steps and the value of the objective function, respectively. According to the curves presented in Fig. 10a, the objective functions are simultaneously reduced as the increase of iterative steps for SGTHB-ITO-MMC, and the SGTHB-ITO-MMC with $m = 3$ and $m = 2$ reduce the iteration steps by 7.33% and 36.00% than the one with $m = \infty$, respectively. Moreover, the variations in the number of DOFs are depicted in Fig. 10b, which indicates that stricter suitably constraint leads to a significant increase in DOFs. However, due to the significant reduction in iterations at the stage with the hierarchies equaling four levels for SGHTB-ITO-MMC with $m = 2$, the increase in computational effort is very limited for the increased DOFs. Therefore, it is concluded that imposing suitably graded constraints is very necessary to implement the adaptive explicit ITO method in terms of both the convergence rate and numerical robustness.

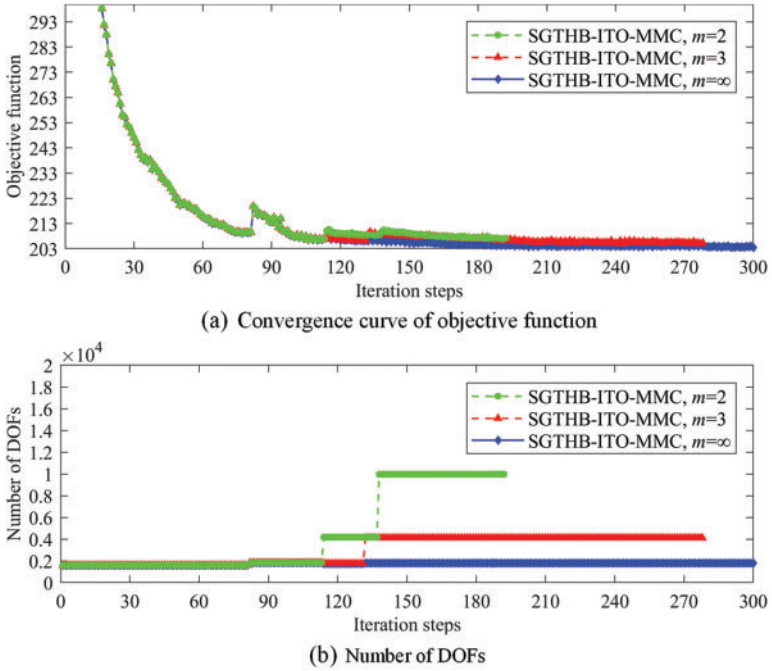

Figure 10: Convergence curve of the objective function and the variations of the number of DOFs for SGTHB-ITO-MMC with $m = 2$, $m = 3$, and $m = \infty$: (a) Convergence curve of the objective function; (b) Number of DOFs

For validating the effectiveness of the improved TDF calculation strategy described in Section 3.3, this work applies it to SGTHB-ITO-MMC with $m = 2$. The optimized structures are depicted in Fig. 11 for the SGTHB-ITO-MMC with or without using the proposed improved TDF calculation strategy. Compared with SGTHB-ITO-MMC without using the improved TDF calculation strategy, the number of iteration steps and DOFs are reduced by 9.38% and 12.36% by applying the improved TDF calculation strategy to SGTHB-ITO-MMC, without altering the objective function and the final converged structure. It can be observed that with the use of the improved TDF calculation strategy, the dense mesh disappears away from the structural boundaries as shown in the red box in Fig. 11, which contributes to reducing the number of DOFs and improving the optimization efficiency. Fig. 12 illustrates the variations of the objective function and the TDF calculation time during the optimization process of SGTHB-ITO-MMC using an improved TDF calculation strategy or not.

According to the results presented in Fig. 12a, the number of iterative steps for SGTHB-ITO-MMC is reduced by 9.38%, and the total TDF calculation time is decreased by 76.29% when the improved TDF calculation strategy is used. In Fig. 12b, the calculation time has abruptly changed at the 80-th, 110-th, 124-th, and 146-th, which is caused by the fact that the TDF values on Gaussian quadrature of all active cells should be calculated to determine the marked cells when the hierarchical mesh is required to be altered, and the improved TDF calculation strategy is triggered to reduce the calculation time once the adaptivity of the hierarchical mesh is finished. Therefore, the proposed improved TDF calculation strategy has a positive impact on SGTHB-ITO-MMC in both convergence rate and optimization efficiency.

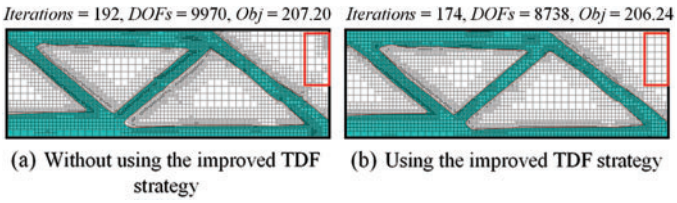

Figure 11: Comparisons of the optimized results without using and using the improved TDF calculation strategy for SGTHB-ITO-MMC: (a) Without using the improved TDF strategy; (b) Using the improved TDF strategy

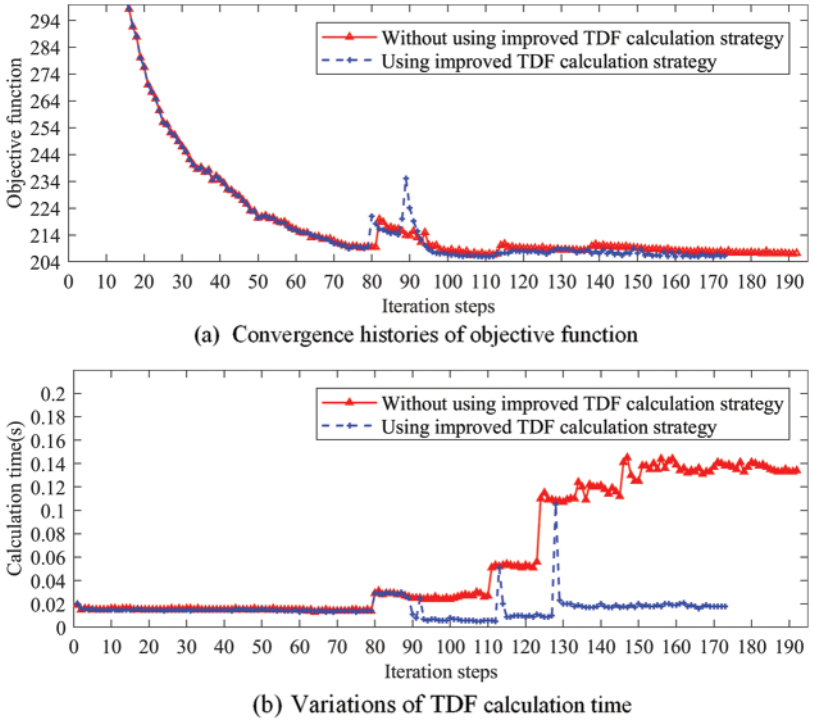

Figure 12: Optimization process of between without using and using the improved TDF strategy: (a) Convergence histories of the objective function; (b) Variations of TDF calculation time

5.2 Short Beam Problem

This section discusses the effectiveness of the SGTHB-ITO-MMC for the short beam and validates the improved TDF calculation strategy under two different dimensionalities of the geometric design space.

5.2.1 Regular Geometric Design Space Case

The problem setting and initial design of MMC are described in Fig. 13. In this problem, the aspect ratio of the design domain is 2:1, which are initially divided into 28 × 14 uniform IGA mesh. The upper limit of the volume fraction is 0.4 for solid material. The maximum number of steps and convergence criteria are identical to those in Section 5.1 "MBB beam problem".

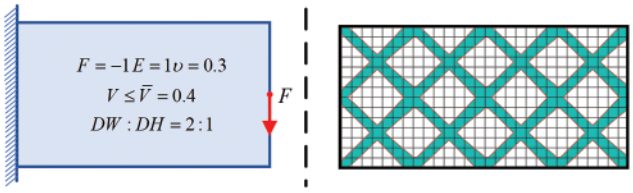

Figure 13: Problem model and initial design for short beam problem

Fig. 14 illustrates the optimized results generated by SGTHB-ITO-MMC with $m = 2$, $m = 3$ and $m = \infty$. It is not difficult to find that the convergence rate of SGTHB-ITO-MMC with $m = 3$ and $m = 2$ are respectively improved by 13.99% and 27.16% than SGTHB-ITO-MMC with $m = \infty$. At the same time, the optimized results exist a tiny hole for SGTHB-ITO-MMC with $m = \infty$ and $m = 3$, which vanishes on the optimal design by SGTHB-ITO-MMC with $m = 2$. Fig. 15 depicts the convergence curves of the objective function for the aforementioned three cases, and it shows the numerical stability of the proposed SGTHB-ITO-MMC method. Finally, the effectiveness of SGTHB-ITO-MMC is verified for the 2D cantilever in a regular geometric design space.

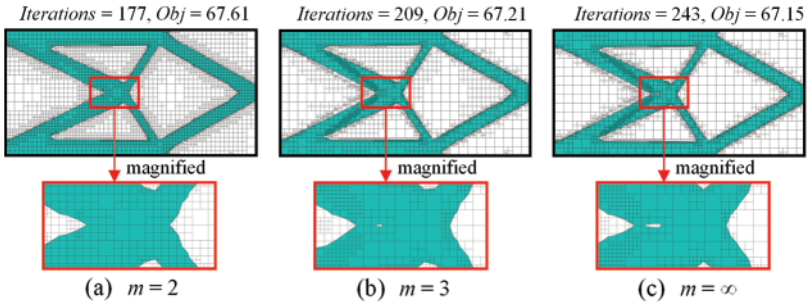

Figure 14: Optimized results by SGTHB-ITO-MMC with (a) $m = 2$, (b) $m = 3$ and (c) $m = \infty$

Fig. 16 illustrates the effect of the improved TDF calculation strategy on the converged results. Using the improved TDF calculation strategy, the number of iteration steps is reduced by 5.65%. The variation curves of the objective function and TDF calculation time are presented in Fig. 17, which show the advantages of the proposed improved TDF calculation strategy in enhancing the convergence rate and the computational efficiency for SGTHB-ITO-MMC. It can be concluded that the improved TDF calculation strategy is valid for the short beam optimized by the SGTHB-ITO-MMC method.

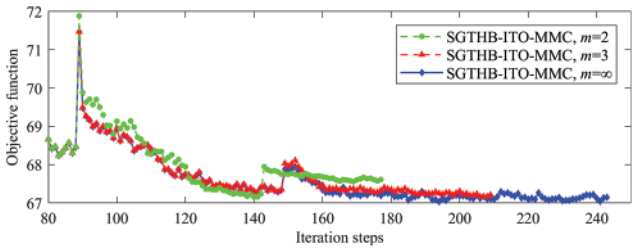

Figure 15: Convergence curve of objective function for short beam for SGTHB-ITO-MMC with $m = 2$, $m = 3$ and $m = \infty$

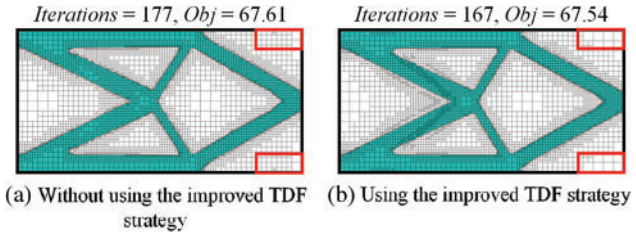

Figure 16: Optimization results of between without using and using the improved TDF strategy: (a) Without using the improved TDF strategy; (b) Using the improved TDF strategy

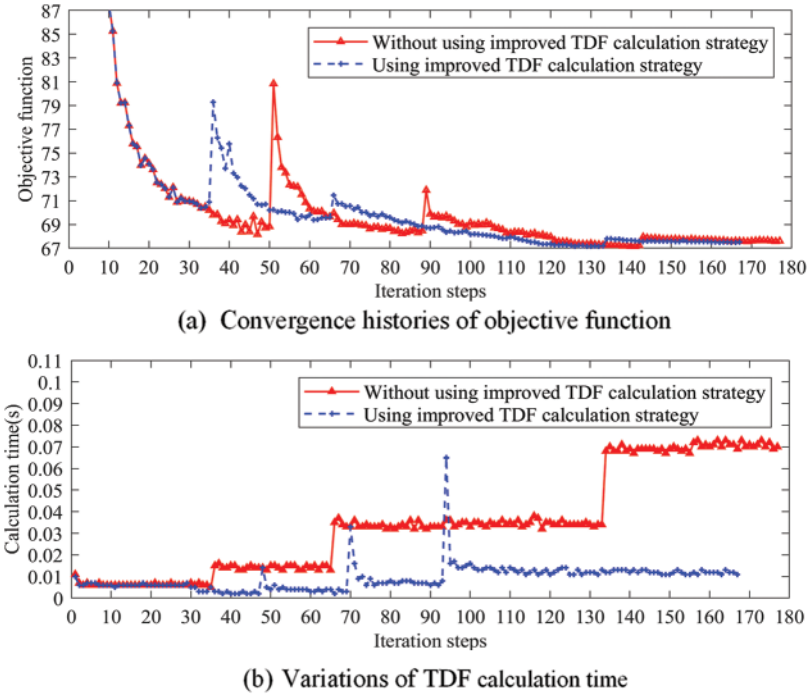

Figure 17: Optimization process of between without using and using the improved TDF strategy: (a) Convergence histories of the objective function; (b) Variations of TDF calculation time

5.2.2 Enlarged Geometric Design Space Case

To verify the effectiveness of the proposed SGTHB-ITO-MMC in an enlarged geometric design space, the initial designs are shown in Fig. 18 for the MMC, with the design domain divided into 4×2 equal sub-regions. During the optimization process, the central coordinates of the MMC must stay in their original sub-regions. The design domain is discretized into 56×28 uniform IGA mesh initially, and the upper limit of volume fraction is 0.4 for solid material. As for the convergence criteria, the one used here is identical to the one presented in Subsection 5.2.1 "Regular geometric design space case", except that the maximum iteration steps are set to 1000.

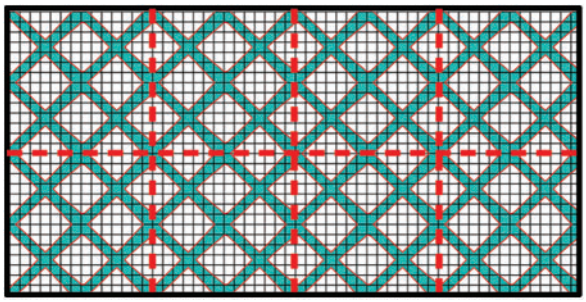

Figure 18: Initial design for the short beam with enlarged geometric design space

Based on the optimized results illustrated in Fig. 19 for SGTHB-ITO-MMC with $m = 2$ and $m = \infty$, the boundaries smoothness and the connections of components are significantly improved by applying the suitably graded constraint with $m = 2$ than these obtained by SGTHB-ITO-MMC without considering suitably graded constraint for hierarchical mesh. Moreover, the convergence histories are compared between $m = 2$ and $m = \infty$, where the number of iterative steps can be reduced from 1000 to 809 by applying the suitably graded constraint. Meanwhile, Fig. 20 expresses the convergence histories are compared between $m = 2$ and $m = \infty$, where the number of iterative steps can be reduced from 1000 to 809. Finally, it finds that the proposed SGTHB-ITO-MMC with $m = 2$ is superior to the one with $m = \infty$ for the enlarged design space, which shows the robustness of the proposed method concerning the dimensionality of the geometric design space.

5.3 3D Cantilever Beam Problem

In this section, the SGTHB-ITO-MMC method is extended to the 3D design problem by taking the 3D cantilever as the last numerical example. As shown in Fig. 21, the left facet of the design domain is fixed and the right bottom side is subjected to a uniform vertical downward line load. To obtain the displacement field, the design domain is initially discretized into $15 \times 15 \times 2$ tri-quadratic IGA elements with the suitably graded constraints taken as $m = 2$ imposed on the hierarchical mesh. The maximum number of steps is 300 and the convergence criterion $\theta_k = \left(\left|C_k - \overline{C}_k\right| / \overline{C}_k\right) \leq 10^{-6}$.

The initial structural components layout for the 3D cantilever, and two intermediate optimized structural layouts, as well as the final convergent result, are shown in Fig. 22, which also includes variations of hierarchical mesh and the convergence process. Under the suitably graded constraints, the boundaries of the 3D cantilever become smoother and the hierarchical mesh is properly graded in the neighborhood of structural boundaries, which verifies the effectiveness of the proposed SGTHB-ITO-MMC method in 3D structural TO problems. In addition, the objective function tends to converge with the increase of the iteration step, and there is no obvious oscillation in the objective function value during the duration of the TO process, which reflects the robustness of the SGTHB-ITO-MMC

method in solving the 3D design problems. These results show that the SGTHB-ITO-MMC method proposed in this work can effectively solve the 3D compliance TO problem.

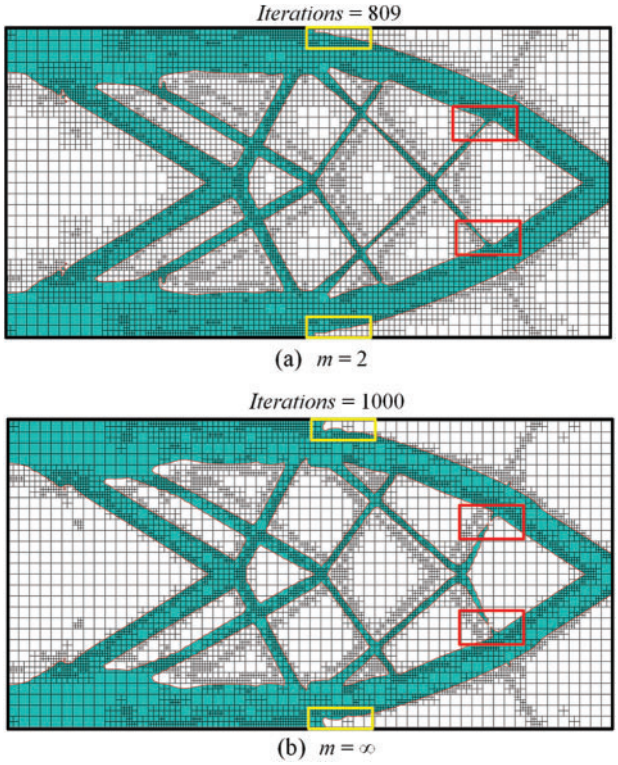

Figure 19: Optimized results by SGTHB-ITO-MMC with (a) $m = 2$ and (b) $m = \infty$ in large geometric design space

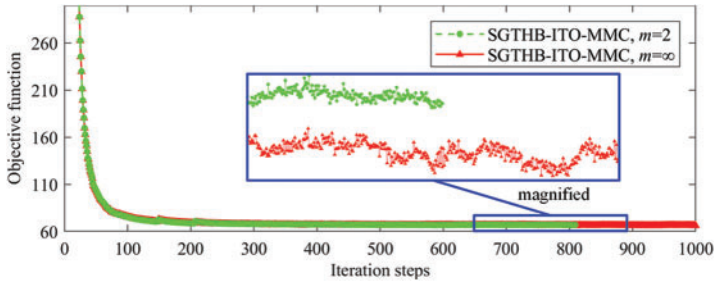

Figure 20: Convergence curve of the objective function for SGTHB-ITO-MMC with $m = 2$ and $\mathrm{m} = \infty$

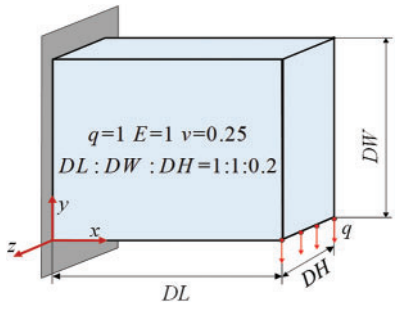

Figure 21: Problem model for 3D cantilever beam problem

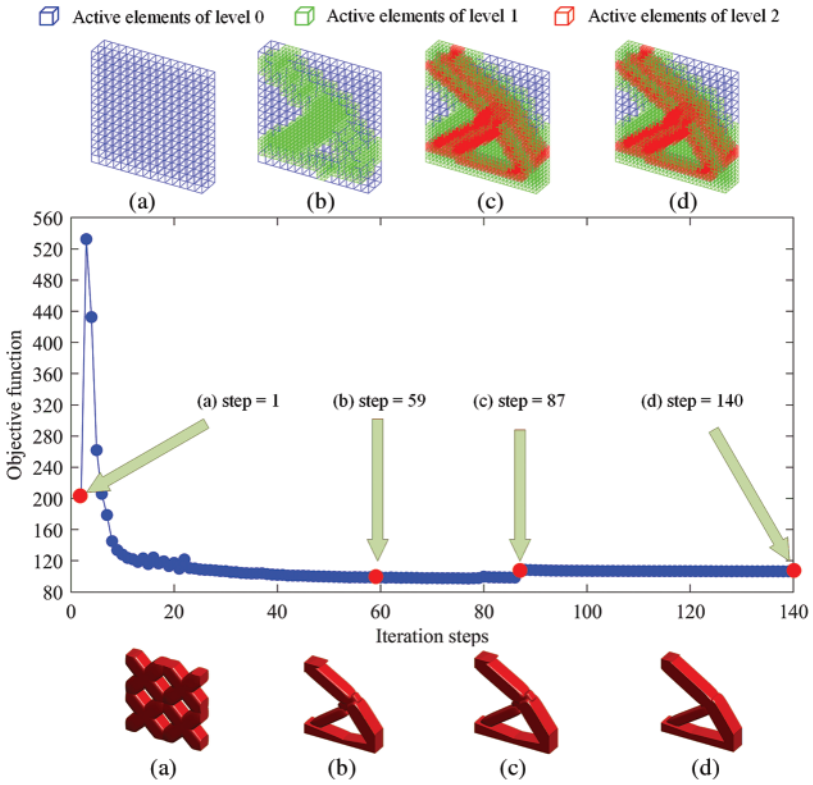

Figure 22: 3D cantilever beam convergence curve in the objective function and optimization process for MMC as well as the variations of hierarchical mesh

6 Conclusions

This work proposes an explicit ITO method in the framework of suitably graded truncated hierarchical B-splines, which is established based on taking the suitably graded constraint into the consideration of the marking strategy. Furthermore, an improved TDF calculation strategy is put forward by reducing the dimensionality of the geometric design space and generating the TDF values locally for the active elements of the hierarchical mesh. By incorporating the suitably graded constraint into the explicit adaptive ITO method, the drawbacks existing in the optimal MMC designs, such as component discontinuities, tiny holes inside the structure, and zigzag boundaries, can be either

eliminated or mitigated to a large extent. Besides, with the stricter suitably graded imposed, the convergence rate of SGTHB-ITO-MMC is increasingly accelerated. With the aid of the proposed improved TDF calculation strategy, the computational efficiency in generating the TDF values and convergence rate are simultaneously improved for SGTHB-ITO-MMC without affecting the optimal designs. Moreover, the proposed method can be applied to 3D design problems.

In the current explicit adaptive ITO method, the versatility is limited by the basic geometric configuration of MMC. To overcome the aforementioned issue, we will extend the current explicit adaptive ITO method to the MMV framework in the future. Furthermore, the stress-constrained problem solved by the adaptive explicit ITO method is also taken as one of our aims.

Funding Statement: This work has been supported by the National Key R&D Program of China (2020YFB1708300) and the Project funded by the China Postdoctoral Science Foundation (2021M701310). The authors would like to thank the anonymous reviewers, whose suggestions helped to substantially improve this manuscript.

Conflicts of Interest: The authors declare that they have no conflicts of interest to report regarding the present study.

References

1. Bendsøe, M. P. (1989). Optimal shape design as a material distribution problem. *Structural Optimization, 1(4),* 193–202. DOI 10.1007/BF01650949.
2. Wang, Y., Sajad, A. K., Michael, T., Damiano, P. (2018). Hip implant design with three-dimensional porous architecture of optimized graded density. *Journal of Mechanical Design, 140(11),* 111406. DOI 10.1115/1.4041208.
3. Xie, Y. M., Steven, G. P. (1993). A simple evolutionary procedure for structural optimization. *Computers & Structures, 49(5),* 885–896. DOI 10.1016/0045-7949(93)90035-C.
4. Xia, L., Zhang, L., Xia, Q., Shi, T. (2018). Stress-based topology optimization using bi-directional evolutionary structural optimization method. *Computer Methods in Applied Mechanics and Engineering, 333(2),* 356–370. DOI 10.1016/j.cma.2018.01.035.
5. Mei, Y., Wang, X. (2004). A level set method for structural topology optimization and its applications. *Advances in Engineering Software, 35(7),* 415–441. DOI 10.1016/j.advengsoft.2004.06.004.
6. Xia, Q., Shi, T. L., Xia, L. (2019). Stable hole nucleation in level set based topology optimization by using the material removal scheme of BESO. *Computer Methods in Applied Mechanics and Engineering, 343(3),* 438–452. DOI 10.1016/j.cma.2018.09.002.
7. Tao, L., Wang, S., Li, B., Gao, L. (2014). A level-set-based topology and shape optimization method for continuum structure under geometric constraints. *Structural and Multidisciplinary Optimization, 50(2),* 253–273. DOI 10.1007/s00158-014-1045-7.
8. Hughes, T. J., Cottrell, J. A., Bazilevs, Y. (2005). Isogeometric analysis: CAD, finite elements, NURBS, exact geometry and mesh refinement. *Computer Methods in Applied Mechanics and Engineering, 194(39–41),* 4135–4195. DOI 10.1016/j.cma.2004.10.008.
9. Qian, X. (2013). Topology optimization in B-spline space. *Computer Methods in Applied Mechanics and Engineering, 265(2),* 15–35. DOI 10.1016/j.cma.2013.06.001.
10. Gao, J., Gao, L., Luo, Z., Li, P. (2019). Isogeometric topology optimization for continuum structures using density distribution function. *International Journal for Numerical Methods in Engineering, 119(10),* 991–1017. DOI 10.1002/nme.6081.

11. Wang, Y., Liao, Z., Ye, M., Zhang, Y., Li, W. et al. (2020). An efficient isogeometric topology optimization using multilevel mesh, MGCG and local-update strategy. *Advances in Engineering Software, 139(8),* 102733. DOI 10.1016/j.advengsoft.2019.102733.
12. Yu, C., Wang, Q., Mei, C., Xia, Z. (2020). Multiscale isogeometric topology optimization with unified structural skeleton. *Computer Modeling in Engineering & Sciences, 122(3),* 779–804. DOI 10.32604/cmes.2020.09363.
13. Zhao, G., Yang, J., Wang, W., Zhang, Y., Du, X. et al. (2020). T-splines based isogeometric topology optimization with arbitrarily shaped design domains. *Computer Modeling in Engineering & Sciences, 123(3),* 1033–1059. DOI 10.32604/cmes.2020.09920.
14. Chen, L., Lu, C., Lian, H., Liu, Z., Zhao, W. et al. (2020). Acoustic topology optimization of sound absorbing materials directly from subdivision surfaces with isogeometric boundary element methods. *Computer Methods in Applied Mechanics and Engineering, 362(3–5),* 112806. DOI 10.1016/j.cma.2019.112806.
15. Chen, L., Lian, H., Natarajan, S., Zhao, W., Chen, Y. et al. (2022). Multi-frequency acoustic topology optimization of sound-absorption materials with isogeometric boundary element methods accelerated by frequency-decoupling and model order reduction techniques. *Computer Methods in Applied Mechanics and Engineering, 395(4),* 114997. DOI 10.1016/j.cma.2022.114997.
16. Guo, X., Zhang, W., Zhong, W. (2014). Doing topology optimization explicitly and geometrically—A new moving morphable components based framework. *Journal of Applied Mechanics, 81(8),* 197. DOI 10.1115/1.4027609.
17. Zhang, W., Chen, J., Zhu, X., Zhou, J., Xue, D. et al. (2017). Explicit three dimensional topology optimization via moving morphable void (MMV) approach. *Computer Methods in Applied Mechanics and Engineering, 322(1),* 590–614. DOI 10.1016/j.cma.2017.05.002.
18. Hou, W., Gai, Y., Zhu, X., Wang, X., Zhao, C. et al. (2017). Explicit isogeometric topology optimization using moving morphable components. *Computer Methods in Applied Mechanics and Engineering, 326(1),* 694–712. DOI 10.1016/j.cma.2017.08.021.
19. Du, B., Zhao, Y., Yao, W., Wang, X., Huo, S. (2020). Multiresolution isogeometric topology optimisation using moving morphable voids. *Computer Modeling in Engineering & Sciences, 122(3),* 1119–1140. DOI 10.32604/cmes.2020.08859.
20. Gai, Y., Zhu, X., Zhang, Y. J., Hou, W., Hu, P. (2020). Explicit isogeometric topology optimization based on moving morphable voids with closed B-spline boundary curves. *Structural and Multidisciplinary Optimization, 61(3),* 963–982. DOI 10.1007/s00158-019-02398-1.
21. Zhang, W., Jiang, S., Liu, C., Li, D., Kang, P. et al. (2020). Stress-related topology optimization of shell structures using IGA/TSA-based moving morphable void (MMV) approach. *Computer Methods in Applied Mechanics and Engineering, 366,* 113036. DOI 10.1016/j.cma.2020.113036.
22. Pan, M., Jüttler, B., Mantzaflaris, A. (2021). Efficient matrix assembly in isogeometric analysis with hierarchical B-splines. *Journal of Computational and Applied Mathematics, 390(39–41),* 113278. DOI 10.1016/j.cam.2020.113278.
23. Patrizi, F., Manni, C., Pelosi, F., Speleers, H. (2020). Adaptive refinement with locally linearly independent LR B-splines: Theory and applications. *Computer Methods in Applied Mechanics and Engineering, 369,* 113230. DOI 10.1016/j.cma.2020.113230.
24. Giannelli, C., Kanduč, T., Pelosi, F., Speleers, H. (2019). An immersed-isogeometric model: Application to linear elasticity and implementation with THBox-splines. *Journal of Computational and Applied Mathematics, 349,* 410–423. DOI 10.1016/j.cam.2018.09.027.
25. Hennig, P., Müller, S., Kästner, M. (2016). Bézier extraction and adaptive refinement of truncated hierarchical NURBS. *Computer Methods in Applied Mechanics and Engineering, 305(39–41),* 316–339. DOI 10.1016/j.cma.2016.03.009.

26. Noël, L., Schmidt, M., Messe, C., Evans, J. A., Maute, K. (2020). Adaptive level set topology optimization using hierarchical B-splines. *Structural and Multidisciplinary Optimization, 62(4),* 1669–1699. DOI 10.1007/s00158-020-02584-6.
27. Xie, X., Wang, S., Xu, M., Jiang, N., Wang, Y. (2020). A hierarchical spline based isogeometric topology optimization using moving morphable components. *Computer Methods in Applied Mechanics and Engineering, 360(2),* 112696. DOI 10.1016/j.cma.2019.112696.
28. Scott, M. A., Thomas, D. C., Evans, E. J. (2014). Isogeometric spline forests. *Computer Methods in Applied Mechanics and Engineering, 269(4),* 222–264. DOI 10.1016/j.cma.2013.10.024.
29. Xie, X., Yang, A., Wang, Y., Jiang, N., Wang, S. (2021). Fully adaptive isogeometric topology optimization using MMC based on truncated hierarchical B-splines. *Structural and Multidisciplinary Optimization, 63(6),* 2869–2887. DOI 10.1007/s00158-021-02850-1.
30. Carraturo, M., Giannelli, C., Reali, A., Vázquez, R. (2019). Suitably graded THB-spline refinement and coarsening: Towards an adaptive isogeometric analysis of additive manufacturing processes. *Computer Methods in Applied Mechanics and Engineering, 348(39),* 660–679. DOI 10.1016/j.cma.2019.01.044.
31. Xie, X., Yang, A., Jiang, N., Wang, S. (2021). Topology optimization using fully adaptive truncated hierarchical B-splines. *Applied Mathematical Modelling, 96,* 131–151. DOI 10.1016/j.apm.2021.02.005.
32. Giannelli, C., Jüttler, B., Speleers, H. (2012). THB-splines: The truncated basis for hierarchical splines. *Computer Aided Geometric Design, 29(7),* 485–498. DOI 10.1016/j.cagd.2012.03.025.
33. Bracco, C., Giannelli, C., Vázquez, R. (2018). Refinement algorithms for adaptive isogeometric methods with hierarchical splines. *Axioms, 7(3),* 43. DOI 10.3390/axioms7030043.